Acta. Chim. Asiana., 2026, 9(1), 795 –802
e-ISSN/p-ISSN 2550-0503/2550-049x
Available online at: www.aca.unram.ac.id

RESEARCH PAPER

Materials modeling of Ge-based nanostructure through metalloid/metal group 13 adsorption compared to Li in ion batteries: monitoring density of states for structural, physical and electronic properties analysis

Fatemeh Mollaamin*
Department of Biomedical Engineering, Faculty of Engineering and Architecture, Kastamonu University, Kastamonu, Turkey.

e-mail: fmollaamin@kastamonu.edu.tr

DOI: https://doi.org/10.29303/aca.v9i1.300

Article info:

Received 06/01/2026

Revised 02/04/2026

Accepted 22/05/2026

Available online 31/05/2026

Abstract: Boron group-based materials, with impressive capacity utilization and self-healing ability, provide better alternatives for alkali metal ion batteries that exhibit all-round performance with the balance of energy/power density and cycling stability. Germanium carbide (GeC) has been designed and characterized as an anode electrode for lithium (Li), boron (B), aluminum (Al) and gallium (Ga)-ion batteries due to forming X_2(GeC) (X = Li, B, Al, Ga) nanoclusters. A vast study on energy-saving by X_2(GeC) complexes was probed using computational approaches due to density state analysis of charge density differences (CDD), total density of states (TDOS) and molecular electrostatic potential (ESP) for hybrid clusters of X_2(GeC). A small portion of Li, B, Al or Ga entered the Ge–C layer could improve the structural stability of the electrode material at high multiplicity, thereby improving the capacity retention rate. Higher Ge/C content can increase battery capacity through X_2(GeC) nanoclusters for energy storage process and improve the rate performances by enhancing electrical conductivity. Besides, GeC anode material may advance cycling consistency by excluding electrode decline and augments the capacity owing to higher surface capacitive impacts. In this research article, the recent progress of boron, aluminum or gallium -based anodes and their storage mechanism is presented.

Keywords: Boron group, germanium carbide, energy-saving, novel hybrid-ion batteries, density of states

Citation: Mollaamin, F. Materials modeling of ge-based nanostructure through metalloid/metal group 13 adsorption compared to li in ion batteries: monitoring density of states for structural, physical and electronic properties analysis . *Acta Chimica Asiana*, *9*(1), 795–802. https://doi.org/10.29303/aca.v9i1.300

INTRODUCTION

Large volume variation during charge/discharge of silicon nanostructures applied as the anode electrodes for high energy lithium-ion batteries (LIBs) has been considered the most critical problem, inhibiting their commercial applications. Searching for alternative high-performance anodes for LIBs has been emphasized. Germanium (Ge), a promising electrode material for high-capacity lithium-ion batteries (LIBs) anodes, attracted much attention because of its large capacity and remarkably fast charge/discharge kinetics. Multivalent-ion batteries are of interest as potential alternatives to LIBs because they have a higher energy density and are less prone to safety hazards. Based on the semiconductor characteristic, Ge has been utilized in semiconductors, catalysts, optical fibers, and sensors [1–5]. Ge has been also extended to the field of lithium-ion batteries (LIBs) because of the rapid advancement of science and technology [6–8].

Germanium-based anodes have good cycling stability and excellent performance due to their high Li^+ diffusivity and electronic conductivity. Compared with other IV group element, germanium anode materials have many unique features. Germanium-based materials with extremely high theoretical energy capacities have gained a lot of attention recently as potential anodes for lithium-ion batteries. These

materials can also offer improved Li insertion/extraction kinetics and cycling performance, providing a promising candidate of anode to meet the increasing demand for batteries with higher energy and power densities [9].

It is believed that germanium-based anodes could meet the increasing requirements for batteries with high power and energy densities. The histogram of the number of publications reflects the increased interest in germanium-based anodes in general during the last decade [10–12].

Recently, a basic understanding of boron and boron-based materials is first introduced. Subsequently, the recent research progress on the application of boron in each component of the lithium battery (LB) is summarized, aiming to understand the hybrid forms of boron and their potential for use in LB materials. Finally, some new strategies and perspectives on the application of boron in LB materials are proposed. Here, the aim is to provide a clear insight into the study of boron in energy storage materials and contribute to the promotion of further research in this area [13].

In comparison to other alloying anodes, such as non-metals silicon, phosphorus, germanium and even metals tin, bismuth and antimony , gallium anode shows a lower capacity. Nevertheless, with a low melting point of 29.8 ℃ and soft mechanical property, gallium is in liquid form at ambient temperature . The flowing feature of liquid enables an arbitrary deformation of gallium to buffer the volume change during the charging and discharging processes [14].

This investigation wants to delve into the feasibility of X_2(GeC) (X= Li, B, Al, Ga) nanoclusters for energy storage. Therefore, it analyzed the physico-chemical properties of mentioned heteroclusters of X_2(GeC). Following in-depth characterization, samples were measured for their performance correlated with chemical composition variations to legislate their potency for the first time in Li-, B-, Al-, or Ga-batteries.

MATERIALS AND METHODS

Development of the applied Density Functional Theory (DFT) methodology only became notable after W. Kohn and L. J. Sham released their reputable series of equations which are introduced as Kohn-Sham (KS) equations [15].Therefore, the precise exchange energy functional is described by the Kohn–Sham orbitals in lieu of the density which is cited as the indirect density functional. This research has employed the penetration of the hybrid functional of three-parameter basis set of B3LYP (Becke, Lee, Yang, Parr)" within the conception of DFT upon theoretical computations and basis sets of LANL2DZ for metal atoms and 6–311+G (d,p) for other atoms The popular B3LYP (Becke, three-parameter, Lee–Yang–Parr) and exchange-correlation functional [16].
Figure1(a,b,c,d) has shown nanoclusters of X_2(GeC) nanoclusters which can enhance the energy storage in battery cells, transistors or other semiconducting devices. In this investigation, the computations have been launched by Coulomb-attenuating method–(Becke, 3-parameter, Lee-Yang-Parr) [CAM–B3LYP–D3] level of theory with multiplicity of +1 and convergence on RMS density matrix=1.00D-08 and convergence on MAX density matrix=1.00D-06 [17].

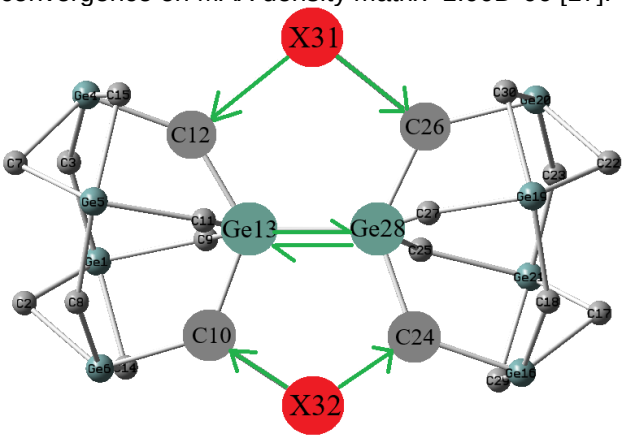

Figure 1. Adding Li, B, Al, Ga to GeC nanocluster and formation of (a) Li_2(GeC), (b) B_2(GeC), (c) Al_2(GeC) and (d) Ga_2(GeC) complexes towards energy storage in novel batteries.

The analysis of Bader charge parameter [18] has been illustrated for energy storage by hybrid clusters of Li_2(GeC), B_2(GeC), Al_2(GeC) and Ga_2(GeC) complexes (Figure1a,b,c,d) due to Gaussian 16 revision C.01 computational software [19] and GaussView 6.1 graphical program [20]. The applied basis sets for theoretical calculations of energy storage by X_2(GeC) complexes has been considered LANL2DZ and 6–311+G (d,p) with multiplicity 1.

One of the most significant advantages of applying GeC nanocluster as the anode in Li, B, Al or Ga batteries is they provide several potential Li/B/Al/ Ga-ion storage ways in a stable GeC anode material, increased electrical conductivity from Ge/C and surface area from the nanocluster morphology. In this investigation, homogenously distributed germanium or carbon elements can be immobilized in the GeC matrix, which prevents their tendency to form agglomeration under battery cycling. The Li/B /Al/ Ga insertion might also result in the cleavage of some C–Li, C–B, C–Al or C–Ga bonds in the GeC anode material and the expansion, providing favorable sites for the subsequent ion insertion in the network (Figure1a,b,c,d). At the same time, the Li, B, Al or Ga atoms could react rapidly with germanium or carbide of GeC nanocluster to form Li_2(GeC) (Figure1a), B_2(GeC) (Figure1b), Al_2(GeC) (Figure1c) and Ga_2(GeC) (Figure1d) heteroclusters. While focusing on B, Al, Ga -based materials to enhance the electrochemical

performance of LBs, we should also explore the theoretical and practical issues involved from the laboratory level to the actual production scale and make a reasonable and comprehensive assessment of the performance of B, Al, Ga-based LBs, to provide guidance for the commercialization of LBs.

RESULTS AND DISCUSSION

Charge density differences analysis

In Figure2(a,b,c,d), charge density differences (CDD) [21] have been shown for X_2(GeC) (X=Li, B, Al, Ga) nanoclusters with the difference density in the district about –12 to +9 Bohr through co-interaction between Li31–Li32, and B31– B32, Al31– Al32, Ga31– Ga32.

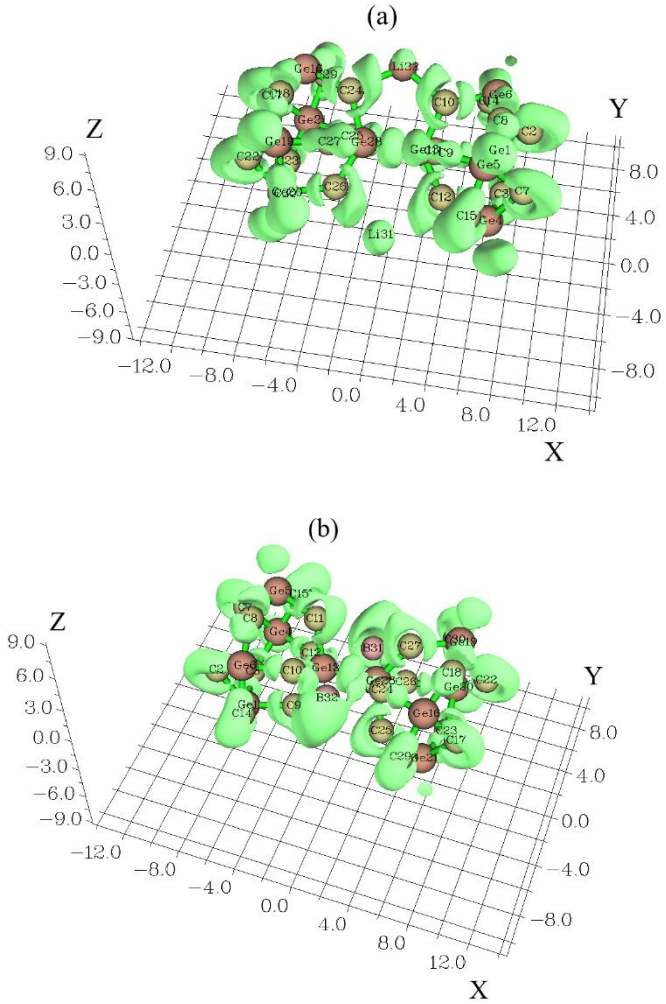

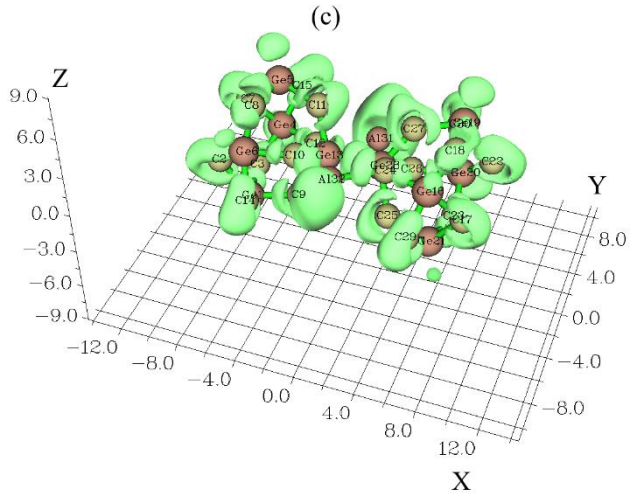

(c) Al_2(GeC) and (d) Ga_2(GeC) nanoclusters. (The unit of X, Y or Z axis is Bohr).

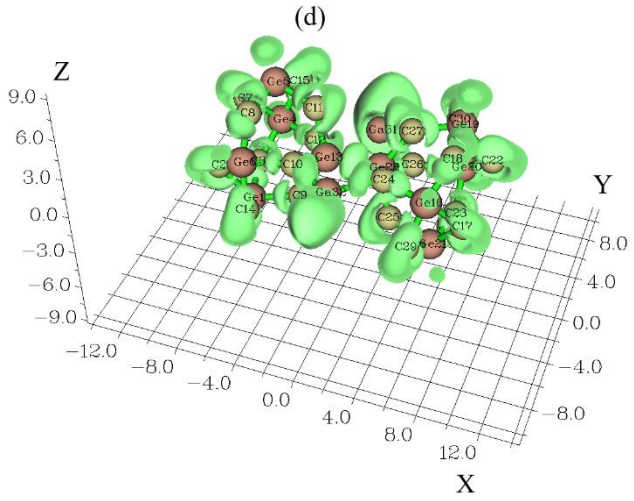

Figure 2. CDD graphs for (a) Li_2(GeC), (b) B_2(GeC),

Moreover, the elements of C2, C3, C7–C12, C14, C15, C17, C18, C22–C27, C29, C30 from X_2(GeC) nanoclusters have displayed the difference density about –12 to +9 Bohr (Figure2a,b,c,d). Functionalizing of Li, B, Al or Ga atoms can augment the negative atomic charge of C2, C3, C7–C12, C14, C15, C17, C18, C22–C27, C29, C30 as electron acceptors in X_2(GeC) nanoclusters.

The charge distribution has been illustrated during atom captured by GeC nanostructure towards formation of X_2(GeC) nanoclusters, respectively (Table1).

Table 1. The atomic charge (Q/coulomb) for X_2(GeC) (X= Li, B, Al, Ga) nanoclusters.

Li_2(GeC)		B_2(GeC)		Al_2(GeC)		Ga_2(GeC)	
Atom	Q	Atom	Q	Atom	Q	Atom	Q
Ge1	0.479	Ge1	0.489	Ge1	0.473	Ge1	0.477
C2	– 0.310	C2	– 0.313	C2	– 0.310	C2	– 0.310
C3	– 0.170	C3	– 0.164	C3	– 0.160	C3	– 0.155
Ge4	0.441	Ge4	0.466	Ge4	0.466	Ge4	0.474
Ge5	0.443	Ge5	0.466	Ge5	0.453	Ge5	0.459
Ge6	0.525	Ge6	0.569	Ge6	0.589	Ge6	0.586
C7	– 0.274	C7	– 0.276	C7	– 0.279	C7	– 0.280
C8	– 0.185	C8	– 0.189	C8	– 0.172	C8	– 0.168
C9	– 0.320	C9	– 0.312	C9	– 0.277	C9	– 0.288
C10	– 0.705	C10	– 0.643	C10	– 1.084	C10	– 1.011
C11	– 0.302	C11	– 0.293	C11	– 0.259	C11	– 0.270
C12	– 0.856	C12	– 0.723	C12	– 0.970	C12	– 0.913
Ge13	1.173	Ge13	1.060	Ge13	1.028	Ge13	1.093
C14	– 0.263	C14	– 0.228	C14	– 0.230	C14	– 0.229
C15	– 0.255	C15	– 0.217	C15	– 0.227	C15	– 0.225
Ge16	0.538	Ge16	0.563	Ge16	0.579	Ge16	0.576
C17	– 0.308	C17	– 0.322	C17	– 0.323	C17	– 0.323
C18	– 0.172	C18	– 0.175	C18	– 0.165	C18	– 0.159
Ge19	0.429	Ge19	0.444	Ge19	0.416	Ge19	0.420
Ge20	0.466	Ge20	0.505	Ge20	0.512	Ge20	0.518
Ge21	0.482	Ge21	0.482	Ge21	0.463	Ge21	0.463
C22	– 0.277	C22	– 0.272	C22	– 0.275	C22	– 0.277
C23	– 0.169	C23	– 0.172	C23	– 0.161	C23	– 0.157
C24	– 0.705	C24	– 0.671	C24	– 1.086	C24	– 1.004
C25	– 0.270	C25	– 0.274	C25	– 0.253	C25	– 0.264
C26	– 0.759	C26	– 0.642	C26	– 0.955	C26	– 0.883
C27	– 0.456	C27	– 0.416	C27	– 0.373	C27	– 0.381
Ge28	1.111	Ge28	0.998	Ge28	1.024	Ge28	1.063
C29	– 0.286	C29	– 0.206	C29	– 0.233	C29	– 0.226
C30	– 0.257	C30	– 0.228	C30	– 0.240	C30	– 0.237
Li31	0.715	B31	0.379	Al31	0.902	Ga31	0.726
Li32	0.500	B32	0.319	Al32	1.129	Ga32	0.909

An algorithm existed for doing decomposition of electronic charge density into atomic contributions. As recommended by Bader, space is divided up into atomic zones where the dividing surfaces are at a minimum in the charge density and the gradient of the charge density is zero along the surface. Instead of indicating the dividing surfaces, the algorithm allocates each point on a regular x, y, z grid to one of the zones (Figure 3a,b,c,d) [22].

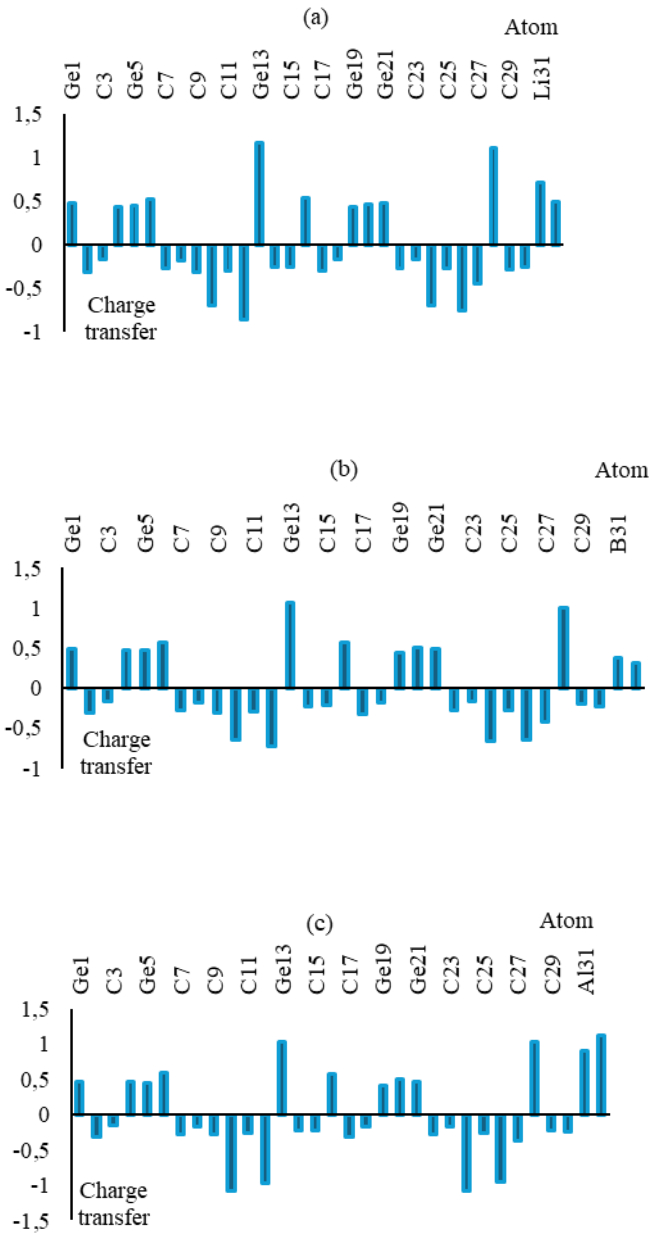

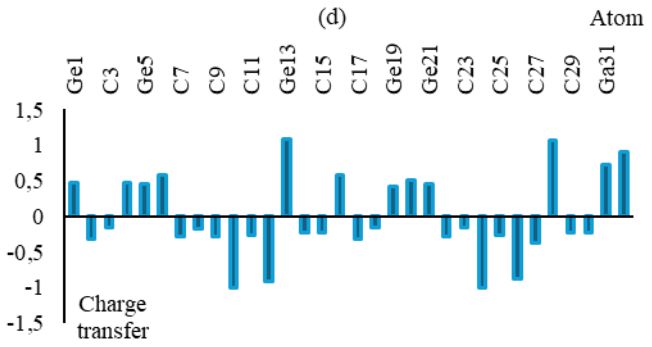

Figure 3. The changes of charge distribution for (a) $Li_2(GeC)$, (b) $B_2(GeC)$, (c) $Al_2(GeC)$ and (d) $Ga_2(GeC)$ nanoclusters.

Total Density of States

In the total density of states "TDOS map", each discrete vertical line corresponds to a "molecular orbital (MO)", the dashed line highlights the position of "HOMO". The curve is the "TDOS" simulated based on the distribution of "MO" energy levels (Figure4a,b,c,d) [23].

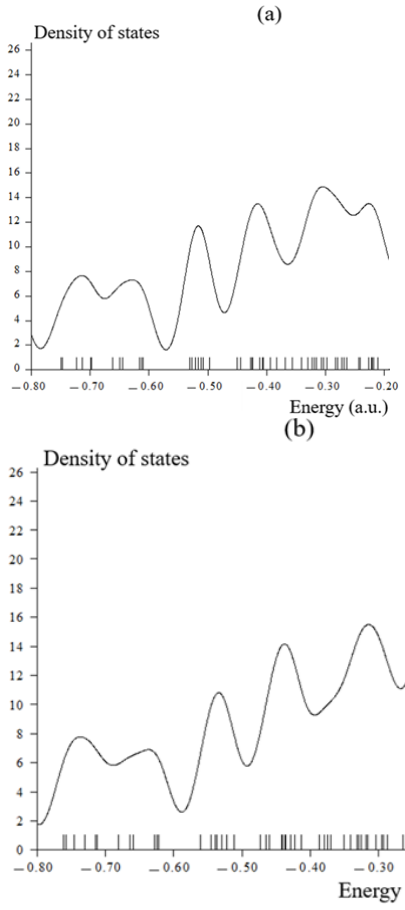

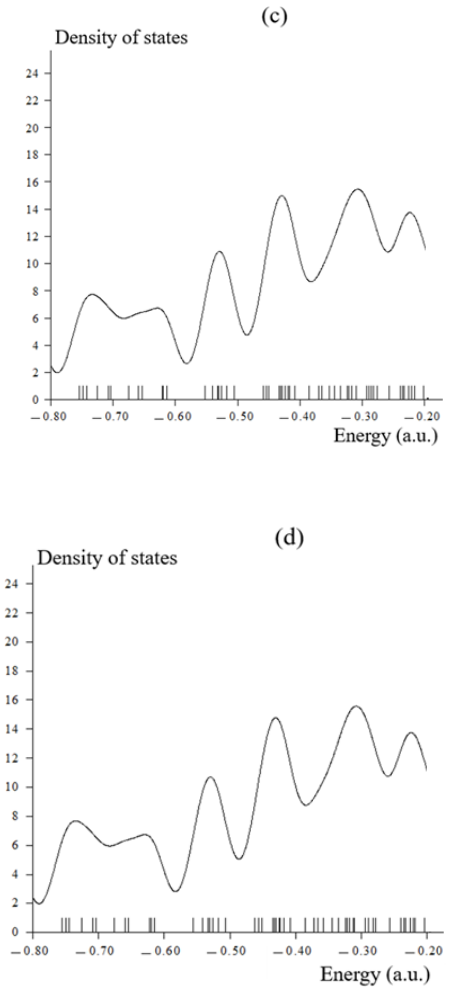

Figure 4. TDOS graph of (a) $Li_2(GeC)$, (b) $B_2(GeC)$, (c) $Al_2(GeC)$ and (d) $Ga_2(GeC)$ nanoclusters.

$X_2(GeC)$ nanoclusters (Figure4a,b,c,d) have shown the steepest maximums TDOS surrounding –0.30, –0.40, –0.50 and –0.60 a.u. owing to covalent bond between Li, B, Al, Ga atoms and GeC nanostructure with maximum density of states of ≈ 12. Substitution engineering is an effective modification strategy to enhance the electrochemical performance of electrode materials. In this investigation, the impacts of heteroatom decorating in GeC nanocluster by substituting the Li atom with the heteroatoms (B, Al, Ga) on the adsorption of main group metals have been systematically investigated using first-principles calculations to evaluate the material performance for application in metal-ion batteries. Therefore, monolayer GeC with heteroatom doping can be applied as a potential anode for metal-ion batteries. This research can clarify the effects of heteroatom decorating and design high performance electrodes for rechargeable batteries.

Molecular electrostatic potential (ESP)

Molecular electrostatic potential (ESP) has been widely used for prediction of nucleophilic and electrophilic sites for a long time. It is also valuable in studying hydrogen bonds, halogen bonds, molecular recognitions and the intermolecular interaction of aromatics [24]. Furthermore, ESP in Multiwfn [25,26] is evaluated exactly by attractive nuclear integrals rather than using approximate methods (such as multipole expansion, numerical Poisson equation), hence you may find the results generated by Multiwfn [25,26] are somewhat different from those outputted by other quantum chemistry codes. In order to speed up ESP evaluation, Multiwfn ignores some integrals that have little contributions. The threshold for ignoring is controlled by "esppreciutoff" in settings.ini, enlarging this parameter results in more accurate ESP value, but also brings more computational cost. The ESP evaluated under default value is accurate enough in general cases.

Trapping of Li, B, Al, Ga atoms by GeC nanostructure (Figure5a,b,c,d) towards formation of X_2(GeC) nanoclusters might be described by ESP graphs using Multiwfn [25,26] due to achieving their delocalization/localization characterizations [27] of electrons and chemical bonds (Figure5a,b,c,d).

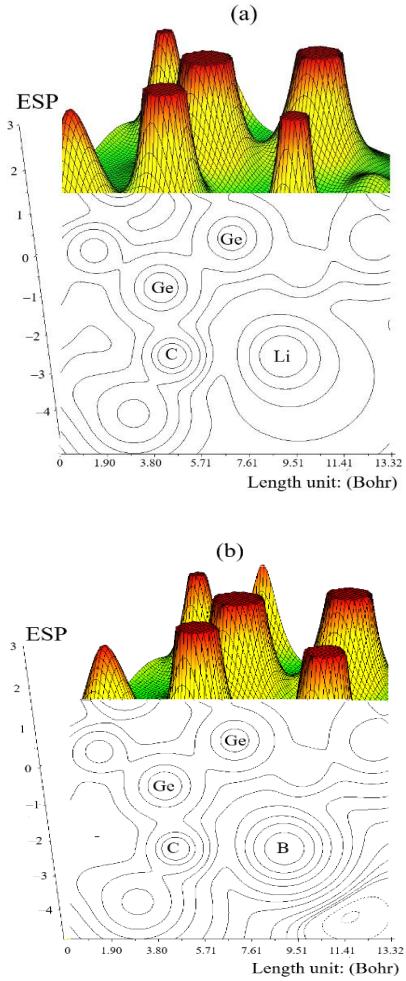

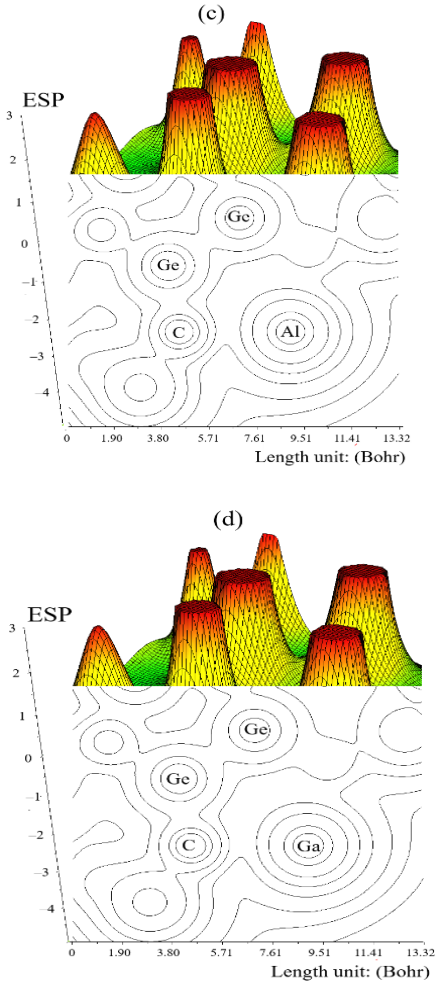

Figure 5. The ESP map for (a) Li_2(GeC), (b) B_2(GeC), (c) Al_2(GeC) and (d) Ga_2(GeC) nanoclusters.

Li_2(GeC) (Figure5a), B_2(GeC) (Figure5b), Al_2(GeC) (Figure5c), Ga_2(GeC) (Figure5d) have demonstrated the electron delocalization through an isosurface map with labeling atoms of C10, C12, Si13, C24, C26, Si28, X31/X32 (X=Li, B, Al, Ga). In fact, the counter map of ESP can confirm that Li_2(GeC), B_2(GeC), Al_2(GeC) and Ga_2(GeC) nanoclusters may augment the efficiency of energy storage (Figure5a,b,c,d).

Besides, intermolecular orbital overlap integral is important in illustration of intermolecular charge transfer which can compute HOMO-HOMO and LUMO-LUMO overlap integrals between Li, B, Al, Ga atoms and GeC nanostructure. The layered germanium carbide improved by lithium, boron, aluminum and gallium have indicated the structural stability of Li-, B-, Al-, and Ga-ion batteries through the reported stability energies in Table 2.

Table2. Stability energy (kcal/mol), dipole moment (debye), LUMO (eV), HOMO(eV), energy gap (ΔE) (eV) and cell capacity (C, mAh g^{-1}) for Li_2(GeC), B_2(GeC), Al_2(GeC) and Ga_2(GeC) nanoclusters.

Heteroclusters	$E_s \times 10^{-3}$ (kcal/mol)	Dipole moment (debye)	E_{HOMO} (eV)	E_{LUMO} (eV)	$\Delta E = E_{LUMO} - E_{HOMO}$ (eV)	C (C, mAh g^{-1})
$Li_2(GeC)$	-507.966	1.118	-5.157	-4.092	1.064	544.076
$B_2(GeC)$	-529.508	0.337	-5.443	-4.490	0.953	1513.338
$Al_2(GeC)$	-500.989	1.259	-5.289	-4.279	1.010	1160.195
$Ga_2(GeC)$	-501.070	1.102	-5.330	-4.284	1.020	717.618

Moreover, intermolecular orbital overlap integral is important in discussions of intermolecular charge transfer which can calculate HOMO-HOMO and LUMO-LUMO overlap integrals between the metal/metalloids and germanium carbide. The wavefunction level we used to be CAM–B3LYP–D3/6–311+G(d,p) that correspond to HOMO and LUMO, respectively (Table2). Therefore, E_{LUMO} (eV), E_{LUMO} (eV) and the local bandgap energies (ΔE/eV) and immobile charges induced by polarization discontinuity are simultaneously controlled throughout the structures, and optimized band profiles are eventually achieved for $X_2(GeC)$ nanoclusters (Table2). A small portion of Li, B, Al or Ga entered the Ge–C layer could improve the structural stability of the electrode material at high multiplicity, thereby improving the capacity retention rate of 100.2018, 94.5295, 198.8630, and 188.1862 $mAhg^{-1}$ for $X_2(GeC)$ complexes, respectively (Table2).

CONCLUSION

To develop the high energy density of LBs and solve such problems as Li dendrites, boron has received significant attention due to its unique advantages, such as the diversity of hybrid forms and molecular structures. Metal/metalloid atom captured by germanium carbide towards formation of $X_2(GeC)$ (X = Li, B, Al, Ga) nanoclusters were studied by computational method. The changes of charge density defined as a notable charge transfer in $X_2(GeC)$. Due to the semiconducting nature of GeC, it is usually composited with C for better ionic and electronic conductivities. It is well established that enhancing Li, B, Al, or Ga to cell batteries can augment the energy-saving in cell batteries. The results of this research article represent that the architectural design of $X_2(GeC)$ can augment the capacity of battery cell. This research article is useful for designing and constructing Li, B, Al, or Ga hybrid batteries with high power density/energy density with excellent cycle stability and will represent a perspective for the industrial application of these hybrid batteries. The improvement of the interfacial properties of LBs is essential in solving the corresponding problems encountered in their further development, so it needs to be studied in depth how to design and optimize the structure of B, Al, Ga-containing electrolyte additives, Li salts, and binder to meet the requirements of long cycle and high voltage conditions.

ACKNOWLEDGEMENTS

The author is grateful to Kastamonu University for completing this paper and its research.

REFERENCES

[1] B.I.N.G. Mingcheng, M.O. Fan, H.U. Zhengfei, Electrochemistry. **88**, 525–531 (2020). doi.org/10.5796/electrochemistry.20-00064

[2] W. Xia, S. Zheng, L. Qiu, et al.,. Polish Journal of Environmental Studies (2025). doi.org/10.15244/pjoes/203046

[3] O.O. Onawumi, J.A. Olaniyan, A.O. Esan, et al., Materials International. **6**, 27 (2024). doi.org/10.33263/Materials63.027

[4] L. Zhou, L. Xie, J. Dai, et al., Asia-Pacific Journal of Chemical Engineering, e70056 (2025). doi.org/10.1002/apj.70056

[5] X. Ma, H. Li, J. Tan, et al., Journal of Magnesium and Alloys, **13**, 1592–1601 (2025). doi.org/10.1016/j.jma.2024.03.010

[6] G. Shao, D.A.H. Hanaor, J.Wang, et al., ACS Appl Mater Interfaces. **12**, 46045–46056 (2020). doi.org/10.1021/acsami.0c12376

[7] I.G. Shaikhiev, N.V. Kraysman, S.V. Sverguzova, Materials International. **7**, 4 (2025). doi.org/10.33263/Materials71.004

[8] V. Ankam, G.Karka, L.G. Reddy, Materials International, **7**, 1 (2025). doi.org/10.33263/Materials71.001

[9] X. Liu, X.-Y.Wu [a], B.Chang, et al., Energy Storage Materials. **30**, 146–169 (2020). https://doi.org/10.1016/j.ensm.2020.05.010

[10] F. Mollaamin, Russ. J. Phys. Chem. B. **19**, 722–736 (2025). doi.org/10.1134/S1990793125700393

[11] F. Mollaamin, BMC Chemistry. **19**, 233 (2025). doi.org/10.1186/s13065-025-01593-0

[12] F. Mollaamin, M. Monajjemi, Russ. J. Phys. Chem. B **18**, 607–623 (2024). doi.org/10.1134/S1990793124020271

[13] L. Ma, J. Tan, Y. Wang, et al., Advanced Energy Materials, **13**, 2300042 (2023). doi.org/10.1002/aenm.202300042

[14] Y. An, Y. Tian, C. Wei, et al., ACS Nano, **13**, 13690–13701(2019). doi.org/10.1021/acsnano.9b06653

[15] W. Kohn, L. J. Sham, Phys. Rev. **140**, 140, A1133- A1138 (1965). doi.org/10.1103/PhysRev.140.A1133

[16] C. Lee, W. Yang, R.G. Parr, Phys Rev B. **37**, 785–789 (1988). doi.org/10.1103/PhysRevB.37.785

[17] A. D. Becke & K. E. Edgecombe, J. Chem. Phys. **92**, 5397–5403 (1990). doi.org/10.1063/1.458517.

[18] G. Henkelman, A. Arnaldsson, H. Jónsson, Computational Materials Science. **36**, 354–360 (2006). doi.org/10.1016/j.commatsci.2005.04.010

[19] M. J. Frisch, G. W. Trucks, H. B. Schlegel, G. E. Scuseria, M. A. Robb, J. R. Cheeseman, G. Scalmani, V. Barone, G. A. Petersson, H. Nakatsuji, X. Li, M. Caricato, A. V. Marenich, J. Bloino, B. G. Janesko, R. Gomperts, B. Mennucci, H. P. Hratchian, J. V. Ortiz, A. F. Izmaylov, J. L. Sonnenberg, D. Williams-Young, F. Ding, F. Lipparini, F. Egidi, J. Goings, B. Peng, A. Petrone, T. Henderson, D. Ranasinghe, V. G. Zakrzewski, J. Gao, N. Rega, G. Zheng, W. Liang, M. Hada, M. Ehara, K. Toyota, R. Fukuda, J. Hasegawa, M. Ishida, T. Nakajima, Y. Honda, O. Kitao, H. Nakai, T. Vreven, K. Throssell, J. A. Montgomery, Jr., J. E. Peralta, F. Ogliaro, M. J. Bearpark, J. J. Heyd, E. N. Brothers, K. N. Kudin, V. N. Staroverov, T. A. Keith, R. Kobayashi, J. Normand, K. Raghavachari, A. P. Rendell, J. C. Burant, S. S. Iyengar, J. Tomasi, M. Cossi, J. M. Millam, M. Klene, C. Adamo, R. Cammi, J. W. Ochterski, R. L. Martin, K. Morokuma, O. Farkas, J. B. Foresman, and D. J. Fox, Gaussian 16, Revision C.01, Gaussian, Inc., Wallingford CT, 2016.

[20] R. Dennington, T. A. Keith, J. M. Millam, GaussView, Version 6.06.16, Semichem Inc., Shawnee Mission, KS, 2016.

[21] Z. Xu, C. Qin, Y. Yu, et al., AIP Advances. **14**, 055114 (2024). doi.org/10.1063/5.0208082

[22] G Henkelman, A Arnaldsson, and H Jónsson, Computational Materials Science. **36**, 354–360 (2006). doi.org/10.1016/j.commatsci.2005.04.010

[23] Z. Rukelj, I. Kupčić, D. Radić, Symmetry. **16**, 38 (2024). doi.org/10.3390/sym16010038

[24] Jane S. Murray, Peter Politzer, The electrostatic potential: an overview. WIREs Comput. Mol. Sci. **1**, 153–163 (2011). https://doi.org/10.1002/wcms.19.

[25] T. Lu & F. Chen, J. Comput. Chem. **33**, 580–592 (2012). doi.org/10.1002/jcc.22885

[26] T. Lu, J. Chem. Phys. **161**, 082503 (2024). doi.org/10.1063/5.0216272

[27] C. F. Matta, P. W. Ayers, R. Cook, Lecture Notes in Chemistry, Springer, Cham, **112** (2024). doi.org/10.1007/978-3-031-51434-0_2.